ADVANCED SENSOR RESEARCH Open Access
www.advsensorres.com

Ultrafast Humidity Sensing Layers Made by Two-Photon Polymerization and Initiated Chemical Vapor Deposition

Stefan Cesnik, Gabriel Hernández Rodríguez, Alexander Bergmann, and Anna Maria Coclite**

Abstract: Humidity sensors are used in many applications. The design of fast sensors that can operate in explosive environments is a difficult task. Therefore, current research efforts aim at combining reliability, sensitivity and high sensing speed. The use of structured ultrathin hydrogels perfectly meets these requirements. Nanostructures are directly fabricated with a two-photon-polymerisation (2PP) 3D printer to use them as templates for hydrogels. After the 3D printing multiple templates are coated with ultrathin films of poly(2-hydroxyethyl-methacrylate) (pHEMA) using initiated chemical vapor deposition (iCVD). p(HEMA) is a humidity responsive hydrogel which changes its thickness by orders of magnitude depending on the ambient conditions. The 3D printed structures are optimized to give both a fast response time, and an optical read-out method for visible wavelengths. Upon hydrogel swelling, the height of the nanostructure pillars increases, keeping their periodicity constant. This induces a change in intensity of the first -order refraction peak, which can be easily measured also at low humidity levels. The humidity response of the nanostructures is measured and an influence for different hydrogel thicknesses and humidity flow rates is observed. The ultrathin film with the lowest thickness of 50 nm shows the fastest response to relative humidity, which is much faster than commercial sensors with 8 s response time.

1. Introduction

Over the past years, measuring the relative humidity established itself to be an important parameter in various fields of application, from industry (e.g., fuel cell applications in the automotive domain, corrosion detection, pulp and paper manufacturing, humidity in bio-gas) to health aspects for the human body.[1,2] According to the current state-of-the-art relative humidity[3] can be measured with different devices: the standard ones are called hygrometers, which quantify the amount of water vapor in the air. Other devices are psychrometer, which measure the temperature difference between a dry and wet bulb, contrary to dew point hygrometer which detect the optical condensation on a chilled surface. Due to their high time consumption gravimetric methods are mostly used for calibration processes.[4] Current state of the art humidity sensors measure the change of the capacity or impedance of polymer films or metal oxide film layer.[5,6]

The processing of the active sensing layer of humidity devices offer a huge potential for advanced research. By direct nanostructuring sensitive polymer thin films using nanoimprint lithography (NIL) our group already showed[7] that the effective sensing area can be increased by optimizing the surface-to-volume ratio, resulting in a faster response compared to state of the art humidity sensors.

In general, the most common techniques to nanostructure hydrogels were reported with templates made of anode aluminum oxide (AAO)[8,9] or nanosphere lithography.[10–13] Hydrogel nanostructures can be fabricated with colloidal lithography.[14] A summary of more lithography based methods[15,16] can be found in literature. Other techniques to directly structure polymer films were reported with femtosecond lasers[17] or electron beam lithography (e-beam).[18,19] However, the latter method is known to be a very time consuming process. Additional methods of structuring polymers can be found in ref. [16, 20–22]. An example for the fabrication of nanoporous micro-structures with initiated chemical vapor deposition (iCVD) can be found in ref. [23]. The main disadvantages of the previous described techniques can be an expensive fabrication, an irregular arrangement of the nanostructures or limitations regarding the area sizes of the nanostructures on a substrate. In addition post treatment of the substrate is often required.

For the present work, we chose a different approach, namely to combine two-photon-polymerisation (2PP) printing with iCVD. Due to the numerous areas in scientific and industrial applications 3D printing is becoming more and more interesting. 2PP

S. Cesnik, A. Bergmann
Inffeldgasse 33 / I, Graz 8010, Austria
E-mail: alexander.bergmann@tugraz.at
G. Hernández Rodríguez, A. M. Coclite
Petersgasse 16, Graz 8010, Austria
E-mail: anna.coclite@tugraz.at

The ORCID identification number(s) for the author(s) of this article can be found under https://doi.org/10.1002/adsr.202200100

DOI: 10.1002/adsr.202200100

presents a very important sub-genre in the 3D printing technology, especially, in the fields of micro- and nano-fabrication. Two-photon-polymerisation printers contain a femtosecond laser which allows to precisely cure small volumes of resin resulting in very high resolution of the printed structures. The principle of two photon absorption and two photon printing is reported in ref. [24]. Furthermore 2PP can be used to print structures from hydrogels directly,[24] comparable to structuring with NIL.[7] Further examples for complex hydrogel structures which are, for example, needed for cell and tissue engineering by 2PP are reported in ref. [25, 26]. 2PP printers offer a high potential to directly print structures on substrates without intermediate steps or post preparation. Therefore, they seem to be a promising tool to make templates for large structured areas with very high resolution. The advantage that 2PP printed structures are mechanically stable makes them very suitable for coating with functional polymer thin films of nanometer thickness. The deposition is done with a well established technique, the so-called iCVD,[27] that shows two main advantages: first, a versatile tool to grow a variety of materials[28] which can be deposited as ultrathin films on nanostructured templates. Second, the deposited thin films can be very conformal and uniform on the nanostructured template. Especially, the study and application of hydrogels attracted interest in recent years. Hydrogels consist of polymeric networks that are able to change their initial thickness by orders of magnitudes when environmental conditions (e.g., temperature, relative humidity or pH value) change.[29] Therefore, they seem to be promising materials as sensing layers in different fields of application. Hydrogel thin films can be deposited via iCVD.[30] In general, based on different polymers compositions iCVD deposited hydrogels can be responsive to humidity,[31] temperature[32,33] or pH-value.[34] From the authors knowledge the combination of 2PP printing with iCVD polymers to make areas of stable nanostructures was not reported so far.

Electrical humidity sensors with fast response times have already been reported.[35] However, one advantage of optical-based sensors is their applicability in explosive environments due to the absence of conductive components in the sensing area. Furthermore, in optical measurement methods the sensor and detector can be separated from each other, which is advantageous for distance measurements. Previous works of our group showed that the combination of poly(2-hydroxyethyl-methacrylate) (p(HEMA)) hydrogels with interference based detection methods works very well.[36] While the previous work[36] was based on a interference measurement setup with planar thin films, this work describes the nanostructuring of such thin films with a template. Again an optical detection method measured the humidity response. The work of Buchberger[36] also highlighted that optical based read out methods showed an almost three times faster response time compared to commercial state-of-the-art humidity sensors.[6] This work deals with the structuring of the hydrogel thin film by 2PP lithography which allows to fabricate large nanostructured templates for ultrathin hydrogels made by iCVD. Compared to direct structuring, the latter method allows to deposit ultrathin (down to 50 nm in this work) hydrogel films, enabling a faster sensor response time due to shorter diffusion times of the water into the hydrogel thin film. For depositing very thin sensing layers on nanostructures iCVD shines with the benefit of being able to deposit very conformal and uniform thin

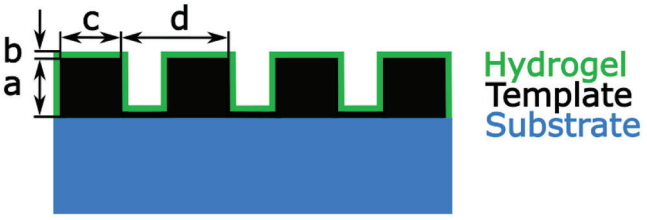

Figure 1. Schematic sketch of the 3D printed nano-template (black) after the ultrathin hydrogel (green) deposition with iCVD and a=3 µm, b=52 nm, 78 nm, 93 nm, c=400 nm, d=800 nm. The dimensions of the glass substrate (blue) is not to scale.

films on the template. This is an advantage, because when the film is thin enough it would prevent the structures from colliding even upon swelling. On the theoretical side we supported the design of the nanostructures with a multi-physic FEM based software. A diffraction grating served as model for the optical part, including the general grating equation:

$$m \cdot \lambda = g \cdot \sin(\Theta_m) \tag{1}$$

with Θ_m being the angle of m-order diffraction peaks, the different wavelengths λ and the grating constant g. Equation 1 describes the position of the peaks but not about the intensity distribution.

2. Results and Discussion

2.1. Fabrication of Nanostructures

The fabrication of nanostructures was done in two steps: first, a template was made with a high resolution and ultrafast 2PP printer. Second, the template was deposited with a thin layer of the humidity responsive hydrogel p(HEMA) using iCVD. Especially important in our case, iCVD offers the great advantage of being able to grow thin films conformally to the trenches in the templates. However, those coated structures could stick together if the layer thickness exceeds the half of the trench size.

Figure 1 shows a SEM picture of the printed 3D grating. In Figure 1a, an overview of the printed area is demonstrated. Here, the concept of printing large nanostructures with 2PP printers is demonstrated: due to limitation in the field of view of the objective the structures are printed in small blocks, which are fitted together afterward. That is also known as stitching and ensures being able to print large areas of nanostructures. A total area of 1.5 mm x 1.5 mm was printed. As shown in Figure 1a, only the lower half of the area was completely covered with the grating. This happened because of a small misalignment of the substrate during the printing process. Figure 1b–d is magnifications of one stitching block of Figure 1a, where the periodic orientation of the lines can be seen. For the current diffraction grating, we printed the lines in one direction. A p(HEMA) hydrogel thin film was deposited on the structure with iCVD as described in Section 4. Figure 1e,f shows SEM images after the iCVD deposition. While Figure 1e was taken normal to the surface, in Figure 1f the samples was tilted. Both figures show that the grating still exists and that the interspaces are not fully filled with p(HEMA), as the layers deposited by iCVD are conformal. Since, the p(HEMA) thin

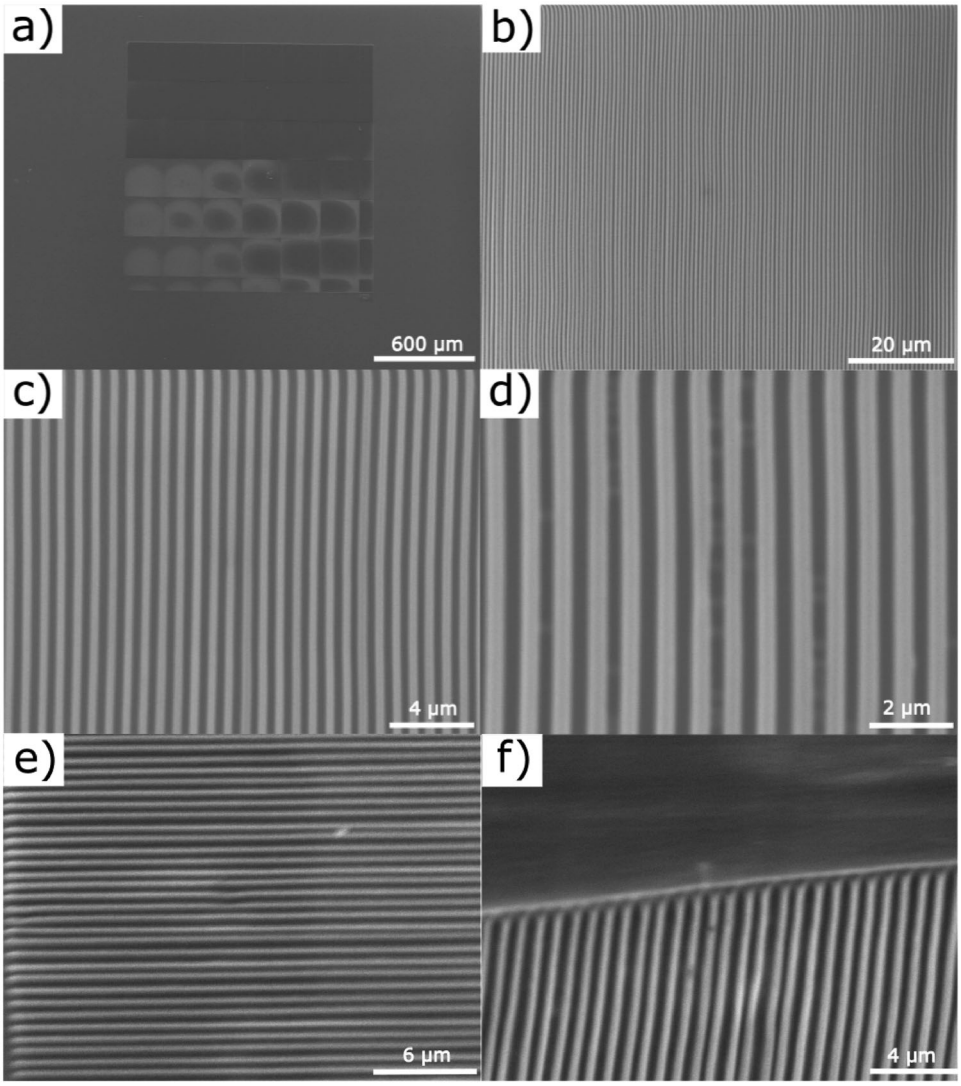

Figure 2. SEM characterization of the 3D printed nanostructure. a–d) Shows the nanotemplate after the fabrication with 2PP. e,f) Shows the nanotemplate coated with the hydrogel.

film has a similar refraction index than the resin, a clear contrast between p(HEMA) and the template was not noticeable. The thin film thickness was measured by ellipsometry and resulted to be: (52± 1), (78± 1), and (93 ± 1) nm. We chose these layer thicknesses to have a good trade off between stability of the deposited thin film nanostructures and improved response time. Figure 1 proves that 2PP printing can be used to make mechanical stable and precisely structured templates. Another advantage of 2PP is that the printed areas can be made relatively large, although increasing the size results in higher costs and larger printing times.

2.2. Humidity Measurement

Figure 2 shows three measurements of the reflected power of the first order (m=1) diffraction peak for changing humidity levels and different layer thicknesses. The measurements were performed with a 635 nm laser and using the setup shown in **Figure 3**. The humidity was changed within the chamber with compressed air and relaxation to ambient humidity afterward. For better visibility the time of opening and closing the valve was added above each subfigure. A commercial sensor (Sensirion SHT-31) was placed inside to simultaneously track the humidity change. In all three Figure 2a–c, the measured reflected power is labeled with red and the commercial sensor with blue. In all Figure 2a–c, a clear correlation between the 2PP hydrogel sensor (red) and the humidity reading of the commercial sensor (blue) is observed: in Figure 2a, the signal of the 2PP hydrogel sensor and the commercial sensor both rise and fall if the humidity increases or decreases, respectively. Contrary, in Figure 2b,c the 2PP hydrogel sensor follows the opposite trend: it rises when the humidity decreases and vice versa. Additionally, in Figure 2c, we notice that the nanostructure humidity sensor shows a very fast humidity response compared to the commercial sensor by comparing the slopes when the relative humidity is dropping. We noticed that for the highest film thickness (Figure 2a),

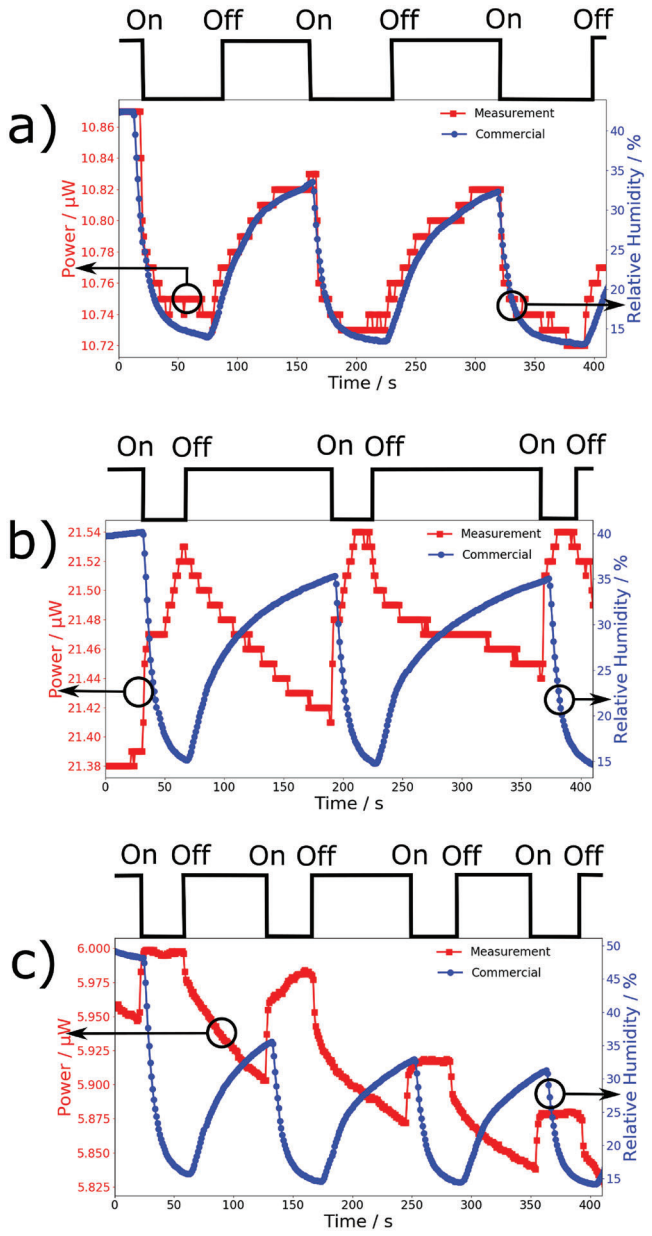

Figure 3. Results of the 2PP hydrogel sensor measurements. The hydrogel thicknesses were 93, 78, and 52 nm for a–c), respectively. "On" and "off" above each subfigure show the time of opening and closing the pressurized air valve. The arrows reference the measurement signals to the respective y-axis.

93 nm thickness) the signal of the 2PP hydrogel sensor followed the signal of the commercial sensor. For both thinner film thicknesses (Figure 2b,c) the 2PP hydrogel sensor was not in phase with the commercial signal anymore, since it was much faster at detecting the rise in humidity. It is also worth to mention that the measurements work exceptionally well for low humidity, although the swelling of the hydrogel is expected to be very small. As shown in the supporting information Figure S2 (Supporting Information) large swellings are detectable only for humidity levels above 80 %. This is due to the optical detection method, which contrarily to other techniques,[37] allows to detect also small thickness changes. For reference, we also performed a measurement on a bare 2PP nanostructured template. The results are reported in Figure S3 (Supporting Information). In this case, no correlation between humidity and power signal can be observed, clearly demonstrating how the humidity response is due to the presence of the hydrogel.

2.3. Simulation Results

The experimental design of nanostructures was supported by multi-physic modeling where the interaction between optical and material properties of the structured hydrogel thin film has been studied. In **Figure 4**, the result of the multiphysic simulation is presented for a single nanopillar coated with the hydrogel, before and after the humidity driven swelling. In the FEM based model we combined the swelling of the hydrogel with the optical properties of the materials and nanostructure in one simulation. Similar to the experiment the optical wave was excited on top and got diffracted by the structure afterward leading to transmitted and reflected light. Due to the structure size and wavelength just diffraction orders of m=−1 and m=+1 were reached. All simulations were done for an incident angle of 0 °. In the optical simulation the results leads to diffraction orders for the direct reflected light (R_0), m=−1 (R_{-1}) and m=+1 (R_{+1}). The diffraction orders of the transmitted light can be seen in the simulation too, but they are not highlighted, because in the experiment the reflected light was measured. The angle of the diffraction orders agrees with the expected angle from the general grating Equation 1.

The results of the swelling simulation of the hydrogel are shown on the right column of Figure 4 and the value of the swelling is included as color bar. For the simulation of the mechanical properties of the ultrathin hydrogel film we used the swelling curve as shown in the supporting information (Figure S3, Supporting Information). In Figure 4b,d,f, the swelling is increased for high humidity. Contrary to Figure 4b,d, we can notice that in Figure 4f the swelling is so strong that it exceeds the boundaries of the unit cell, which could result in sticking of the hydrogel coming from two consecutive pillars for high relative humidity values. The simulations clearly show that the intensity of the diffracted beam increases upon swelling. The diffraction angle of the first order does not change for the swollen ultrathin film. Furthermore, the simulation of the swelling of the hydrogel gives an indication for the maximum thin film deposition thickness.

2.4. Humidity Measurement with Different Flow Rates

In addition, we tried to observe the influence of the humidity flowrate on the hydrogel sensor response to prove that the nanostructured sensor is also sensitive to different change rates of humid air in the measurement chamber. Therefore, the flow rate was controlled with a mass flow controller as shown in Figure 3. We chose the sample with 93 nm layer thickness, because the optical signal showed the best correlation with the commercial sensor and measured the humidity response for the 2PP hydrogel sensor and the commercial sensor for 6, 3, and 0.5 l min^{-1}.

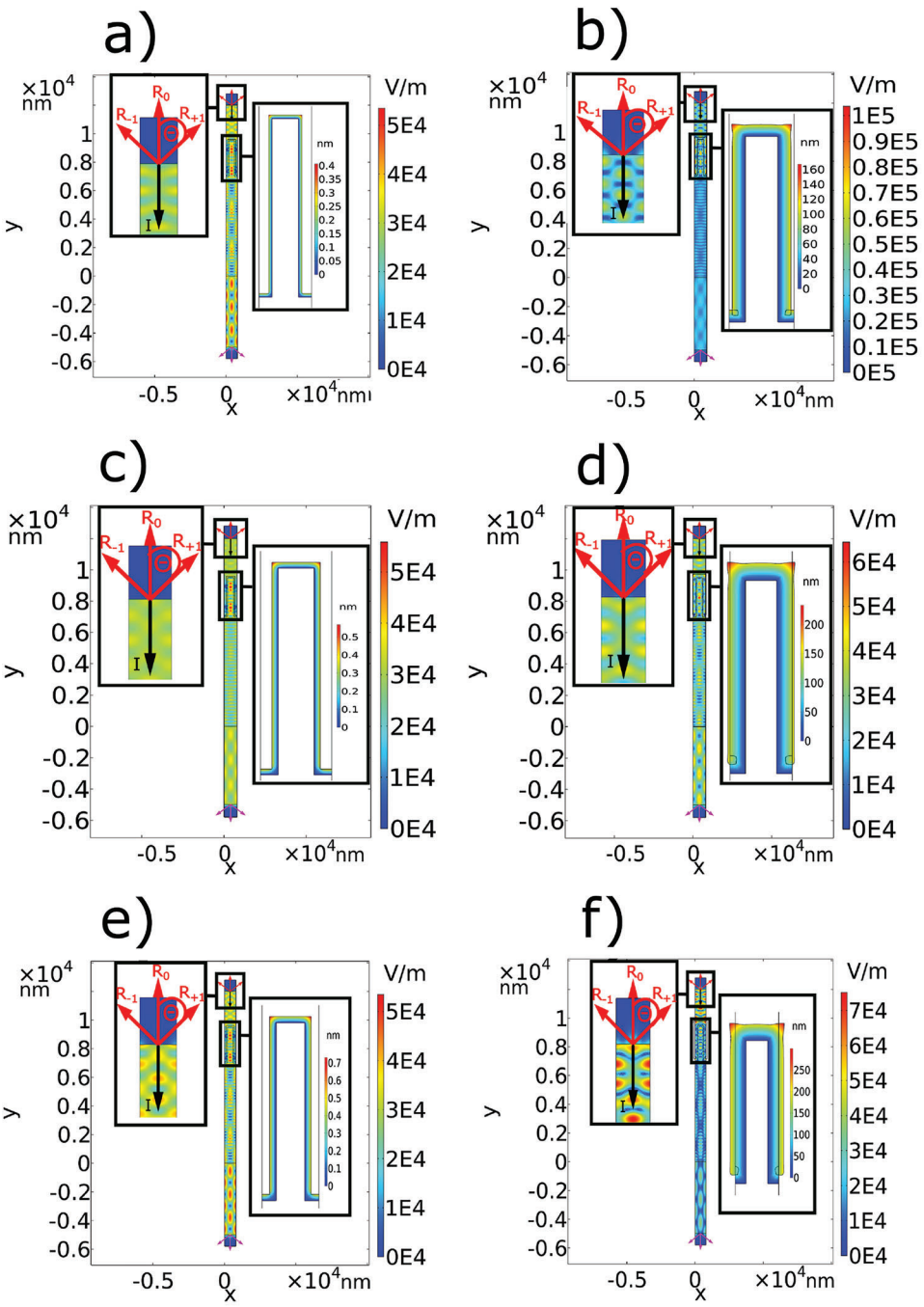

Figure 4. Results of the simulation for low and high swelling of the hydrogel. The simulations in subfigure a,b) were performed for a thin film thickness of 52 nm, subfigure c,d) for 78 nm and finally, e,f) for 93 nm. For better visibility the results of the optical simulation (left column) and the swelling (right column) are magnified in all subfigures. For the optical simulation the color bar indicates the normalized electric field. Abbreviations: R_0... direct reflected beam. R_{-1}... diffraction order m=−1. R_{+1}... diffraction order m=+1. I ... incoming beam.

The result is presented in **Figure 5**: here the reflected power (red) was measured for changing relative humidity, but for different flowrates during one measurement. During the measurement the humidity change was simultaneously measured with a commercial sensor (blue). In Figure 5, the flowrates are marked with colored areas starting from the fastest flowrate (orange, 6 l min^{-1}) to medium (green, 3 l min^{-1}) and slow (violet, 0.5 l min^{-1}). We can observe that the flowrate influences the response behaviour of the measurement signal, leading to faster response times for higher flowrates (orange) by comparing the slopes of the measured signal for different flow rates. Afterward, when changing the flowrate to 0.5 l min^{-1} (violet) the response was much slower. In this experiment the different flowrates influence the supply rate of the humidity within the measurement chamber, therefore

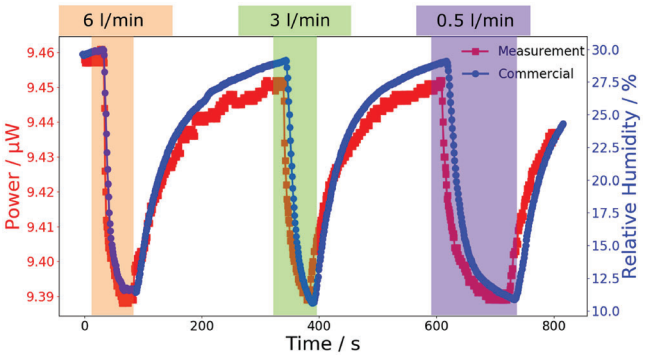

Figure 5. Results of the measurements different humidity flowrates. The colored areas indicate the change of the flowrates: 6 l min^{-1} (orange), 3 l min^{-1} (green), and 0.5 l min^{-1} (violet).

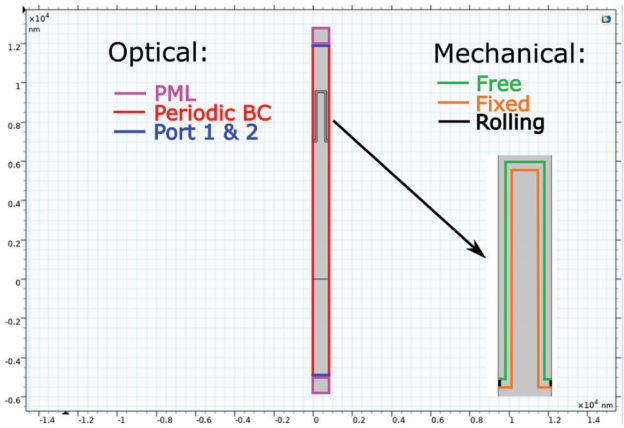

Figure 6. Sketch of the template after the hydrogel deposition.

a higher flowrate results in a faster change of the sensor signal. At low flow rate, when the supply is low, the sensor based on the hydrogel shows a faster response to the humidity then the commercial sensor. Therefore, we conclude that the limiting factor for the humidity measurement speed in the case of the presented devices is the humidity supply. In general, Figure 5 also proves that the the nanostructured thin film dynamically responds for different velocities of humidity changes during one measurement.

3. Conclusion

We demonstrated the combination of p(HEMA) deposited with iCVD and 2PP to fabricate large nanostructured surfaces of ultrathin hydrogels. 2PP printing can be used to fabricate nanotemplates with precise feature sizes down to nanometer length scale. With iCVD we were able to deposit smooth ultrathin films with 52, 78, and 93 nm thickness on 2PP printed templates. Those ultrathin films show very fast response time due to short diffusion times of water into the hydrogel. The nanostructure of the films was designed to measure the intensity the first diffraction order as proxy for humidity. The combination of good optical properties of the ultrathin films together with their great response to the change in humidity made us able to achieve a fast responding 2PP hydrogel sensor. Additionally, an optical readout method allowed to clearly detect changes in the low humidity regime, which was unexpected when using hydrogels as sensing layers due to their lower response in that regime. Compared to the state-of-the-art humidity sensor, which work by electrical read-out and has a response time of around 8 s, the 2PP hydrogel sensor reacted approximately an order of magnitude faster to the change in relative humidity. The 2PP hydrogel sensor also showed different response characteristics depending on the humidity flow rate indicating a fast sensor response. The design and a study about the physical sensor effect was supported by multiphysical simulation in Comsol. Here, we combined the optical and mechanical properties of the thin film. With the optical simulation we were able to simulate the diffraction grating effect, while the mechanical simulation added the swelling of the hydrogel and as well, gave an estimation of the limits for the thicknesses of ultrathin films which are deposited on 2PP templates. COMSOL offers a great tool to support the design of nanostructures and afterward to model the physical effect. The actual model allows to change geometries or parameters very quick to analyze more complex geometries in the future as well. Further work will focus on different template shapes to further optimize the sensor characteristic with respect to stability and rise time.

4. Experimental Section

Modeling of the Nanostructure: The simulation was similarly structured as in previous work[7] and performed with a commercial FEM software (COMSOL). COMSOL brings the advance of multi-physic coupling during one simulation. To reduce the computational time, a unit cell including periodic boundary conditions was designed. Our structure is a diffraction grating, which can be described as a periodic arrangement of lines with different depths. The simulation of the optical properties was done withing the wave optics module, whereas the mechanical properties were simulated with the solid mechanics module. A short summary of the latter module can be found supporting information. In this work, the optical effect causing of the structure design, with the swelling properties of the hydrogel thin film was successfully combined. The utilized materials reproduced the experimental situation as shown in **Figure 6**: On top of the unit cell contains two air regions were build. Inside the second air region were the template and with the hydrogel layer (pHEMA), followed again by two air regions again. The substrate was not considered in the simulation because the different scale compared to the nanostructures would increase the simulation time too much. Figure 6 also shows the different boundary conditions as colored lines, and they will be described in the next subsection:

Wave Optics Module: In Figure 6, the magenta colored boxes are so-called 'Perfectly Matched Layers' (PML) in COMSOL, which were domains to ensure that no electromagnetic waves were reflected back into the ports. The red boundaries show periodic boundary conditions, which were necessary for describing a diffraction grating. For the propagation of electromagnetic waves two ports, namely an excitation port (Port 1) and a transmission port (Port 2), which were both indicated with blue, were needed. The excitation Port 1 also receives the reflected part of the light. The optical simulations were performed with the perfect structure-to-wavelength ratio of the diffraction grating which was, of course, never accomplished in the experimental situation. The wavelength of the incident electromagnetic wave at Port 1 was set to 635 nm, similar to the laser in the experiment.

Hygroscopic Swelling: The swelling was modeled from experimental data which were recorded by in-house ellipsometry (see Supporting Information). The drawn black lines in Figure 6 were called rolling boundary conditions which prevent the hydrogel to swell in the horizontal direction. Contrary, to free boundary conditions (green) that ensure the swelling hydrogel in all directions. Finally, at the interface between template

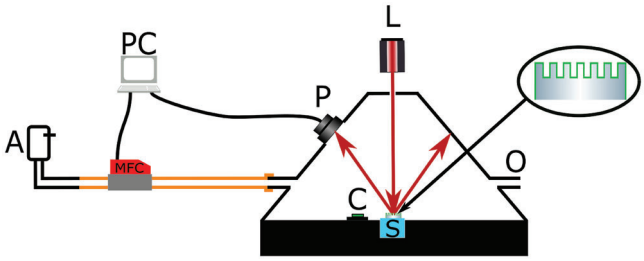

Figure 7. Sketch of the measurement setup with magnified measurement cell. (A) Pressured Air, (MFC) Massflow Controller, (P) Powermeter, (L) Laser, (C) Commercial Sensor, (S) Substrate, and (O) Outlet.

and hydrogel fixed boundary conditions simulated the non-swelling of the template.

Nanotemplate Fabrication: The nanotemplate was fabricated with the 2PP 3D printer NanoOne.[38] The printer contains a femtosecond laser with 250 mW maximum average power, 95 fs pulse length, 780 nm center wavelength and 80 MHz repetition rate. For the current structure dimensions the 60x objective (NA=1.42) was used, being able to reach feature sizes of $\leqslant 200$ and $\leqslant 550$ nm for horizontal and vertical direction, respectively. For the printing material the 2-photon resin UpBrix from upNano was used. The structure was printed onto a glass substrate with 10 mm x 10 mm area. After the printing the sample is put into an acetone bath to remove resin residuals. As nanostructure diffraction gratings with a 800 nm grating constant were fabricated with 400 nm linewidths and 400 nm spacing between them.

Thin Film Deposition: The thin film deposition was done in a custom build reactor as already described in ref. [39]. Polymers of 2-hydroxyethylmethacrylate (HEMA, Sigma Aldrich,flowrate = 0.392 sccm) were deposited on Si-wafers and the 3D printed nano-templates. The Si-wafers with planar deposited thin films were used to measure the thickness of the thin films by laser interference in-situ and ellipsometric measurements (Woolam, M2000 VASE) afterward. As initiator for the polymerization di-tert-butyl peroxide (TBPO, Sigma Aldrich, flowrate = 1 sccm) was used. The monomer HEMA was heated up to 70 °C. The working pressure during the thin film deposition was held at 500 mTorr. The substrate and NiCr filament temperatures were 35 and 300 °C, respectively. A schematic sketch of the template after the hydrogel deposition can be seen in **Figure 7**. Please note that the dimensions of the substrate in the sketch do no fit the real ones. Thin films of different thicknesses were deposited on the nano-templates in different depositions cycles. The different layer thicknesses were regulated by the deposition time.

Humidity Measurement Setup: A sketch of the measurement setup is shown in Figure 7. The measurement setup was designed to measure the reflected power (P) of the first order diffraction (m=1) of the grating. The measurement cell was designed with SolidWorks and afterward 3D printed (Formlabs). It contained the nanostrucutured substrate (S) and additionally, a commercial sensor (C) from sensirion (SHT-31) was placed in the measurement chamber too. With a 635 nm laser (L) the first diffraction order was excited. The in-flow of pressured air (A) was regulated with a massflow controller (MFC) from Voegtlin. The humidity ramp was obtained by opening valve A and allowing pressured air to flow in the chamber and lower the RH. Afterward, the valve A was closed until the system had recovered to atmospheric humidity. The MFC, commercial sensor and powermeter were connected to a PC, controlled and read-out by their standard software.

Statistical Analysis: Statistical analysis was not performed, since for the measurements mostly type B measurement uncertainties were assumed.

Supporting Information

Supporting Information is available from the Wiley Online Library or from the author.

Acknowledgements

This project has received partial funding from the European Union's Horizon 2020 research and innovation programme under grant agreement no. 899349. This project was partial funded within the research project ASSIC (Austrian Smart Systems Integration Research Center), which was funded by the Austrian Federal Ministry for Climate Action, Environment, Energy, Mobility, Innovation, and Technology (BMK), the Austrian Federal Ministry for Digital and Economic Affairs (BMDW), and the co-financing federal provinces Carinthia and Styria. ASSIC was a COMET-Center within the framework of COMET (Competence Centers for Excellent Technologies). The COMET program was managed by the Austrian Research Promotion Agency (FFG).

Conflict of Interest

The authors declare no conflict of interest.

Data Availability Statement

The data that support the findings of this study are available from the corresponding author upon reasonable request.

Keywords

Two-photon-polymerization 3D printing, humidity sensors, hydrogel thin films

Received: December 17, 2022
Revised: March 5, 2023
Published online:

[1] Z. Duan, Y. Jiang, H. Tai, *J. Mater. Chem. C* **2021**, *9*, 14963.
[2] A. V. Arundel, E. M. Sterling, J. H. Biggin, T. D. Sterling, *Environ. Health Perspect.* **1986**, *65*, 351.
[3] Z. Chen, C. Lu, *Sens. Lett.* **2005**, *3*, 274.
[4] C.-Y. Lee, G.-B. Lee, *Sens. Lett.* **2005**, *3*, 1.
[5] H. Farahani, R. Wagiran, M. N. Hamidon, *Sensors* **2014**, *14*, 7881.
[6] F. Weller, D. Keller, S. Wettstein, M. Graf, *Proceedings* **2018**, *2*, 13.
[7] S. Cesnik, A. Perrotta, A. Cian, M. Tormen, A. Bergmann, A. M. Coclite, *Macromol. Rapid Commun.* **2022**, *43*, 2200150.
[8] L. Wen, R. Xu, Y. Mi, Y. Lei, *Nat. Nanotechnol.* **2017**, *12*, 244.
[9] G. O. Ince, G. Demirel, K. K. Gleason, M. C. Demirel, *Soft Matter* **2010**, *6*, 1635.
[10] C. L. Cheung, R. J. Nikolić, C. E. Reinhardt, T. F. Wang, *Nanotechnology* **2006**, *17*, 1339.
[11] P. Colson, C. Henrist, R. Cloots, *J. Nanomaterials* **2013**, 2013.
[12] C. L. Haynes, R. P. Van Duyne, *J. Phys. Chem. B* **2001**, *105*, 5599.
[13] M. Krupinski, M. Perzanowski, A. Maximenko, Y. Zabila, M. Marszałek, *Nanotechnology* **2017**, *28*, 194003.
[14] N. J. Trujillo, S. Baxamusa, K. K. Gleason, *Thin Solid Films* **2009**, *517*, 3615.
[15] Y. Ofir, I. W. Moran, C. Subramani, K. R. Carter, V. M. Rotello, *Adv. Mater.* **2010**, *22*, 3608.
[16] C. Acikgoz, M. A. Hempenius, J. Huskens, G. J. Vancso, *Eur. Polym. J.* **2011**, *47*, 2033.
[17] F. Korte, J. Serbin, J. Koch, A. Egbert, C. Fallnich, A. Ostendorf, B. N. Chichkov, *Appl. Phys. A* **2003**, *77*, 229.
[18] R. Zandi Shafagh, A. Vastesson, W. Guo, W. van der Wijngaart, T. Haraldsson, *ACS Nano* **2018**, *12*, 9940.

[19] W. Yue, Z. Wang, Y. Yang, L. Chen, A. Syed, K. Wong, X. Wang, *J. Micromech. Microeng.* **2012**, *22*, 125007.
[20] S. Nejati, K. K. S. Lau, *Nano Lett.* **2011**, *11*, 419.
[21] D. Li, J. Huang, R. B. Kaner, *Acc. Chem. Res.* **2009**, *42*, 135.
[22] H. D. Tran, D. Li, R. B. Kaner, *Adv. Mater.* **2009**, *21*, 1487.
[23] H. Sojoudi, S. Kim, H. Zhao, R. K. Annavarapu, D. Mariappan, A. J. Hart, G. H. McKinley, K. K. Gleason, *ACS Appl. Mater. Interfaces* **2017**, *9*, 43287.
[24] J.-F. Xing, M.-L. Zheng, X.-M. Duan, *Chem. Soc. Rev.* **2015**, *44*, 5031.
[25] J. Song, C. Michas, C. S. Chen, A. E. White, M. W. Grinstaff, *Adv. Healthcare Mater.* **2020**, *9*, 1901217.
[26] B. S. Calin, I. A. Paun, *Int. J. Mol. Sci.* **2022**, *23*, 22.
[27] W. E. Tenhaeff, K. K. Gleason, *Adv. Funct. Mater.* **2008**, *18*, 979.
[28] S. J. Yu, K. Pak, M. J. Kwak, M. Joo, B. J. Kim, M. S. Oh, J. Baek, H. Park, G. Choi, D. H. Kim, J. Choi, Y. Choi, J. Shin, H. Moon, E. Lee, S. G. Im, *Adv. Eng. Mater.* **2018**, *20*, 1700622.
[29] S. Dwivedi, P. Khatri, G. R. Mehra, V. Kumar, *Int. J. Pharm. Biol. Arch.* **2011**, *2*, 1588.
[30] K. Chan, K. K. Gleason, *Langmuir* **2005**, *21*, 8930.
[31] K. Unger, R. Resel, A. M. Coclite, *Macromol. Chem. Phys.* **2016**, *217*, 2372.
[32] O. Werzer, S. Tumphart, R. Keimel, P. Christian, A. M. Coclite, *Soft Matter* **2019**, *15*, 1853.
[33] F. Muralter, A. M. Coclite, O. Werzer, *J. Phys. Chem. C* **2019**, *123*, 24165.
[34] Z. Zhang, L. Chen, C. Zhao, Y. Bai, M. Deng, H. Shan, X. Zhuang, X. Chen, X. Jing, *Polymer* **2011**, *52*, 676.
[35] S. Taccola, F. Greco, A. Zucca, C. Innocenti, C. de Julián Fernández, G. Campo, C. Sangregorio, B. Mazzolai, V. Mattoli, *ACS Appl. Mater. Interfaces* **2013**, *5*, 6324.
[36] A. Buchberger, S. Peterka, A. M. Coclite, A. Bergmann, *Sensors* **2019**, *19*, 5.
[37] T. Abu Ali, P. Schäffner, M. Belegratis, G. Schider, B. Stadlober, A. M. Coclite, *Adv. Mater. Technol.* **2022**, *7*, 2270038.
[38] M. Luitz, M. Lunzer, A. Goralczyk, M. Mader, S. Bhagwat, A. Warmbold, D. Helmer, F. Kotz, B. E. Rapp, *Adv. Mater.* **2021**, *33*, 2101992.
[39] C. Ranacher, R. Resel, P. Moni, B. Cermenek, V. Hacker, A. M. Coclite, *Macromolecules* **2015**, *48*, 6177.